# Biophysical Model of Ion Transport across Human Respiratory Epithelia Allows Quantification of Ion Permeabilities

Guilherme J. M. Garcia,[†‡*] Richard C. Boucher,[‡] and Timothy C. Elston[†]
[†]Department of Pharmacology and [‡]Cystic Fibrosis/Pulmonary Research and Treatment Center, and the University of North Carolina Virtual Lung Group, University of North Carolina at Chapel Hill, Chapel Hill, North Carolina

ABSTRACT Lung health and normal mucus clearance depend on adequate hydration of airway surfaces. Because transepithelial osmotic gradients drive water flows, sufficient hydration of the airway surface liquid depends on a balance between ion secretion and absorption by respiratory epithelia. In vitro experiments using cultures of primary human nasal epithelia and human bronchial epithelia have established many of the biophysical processes involved in airway surface liquid homeostasis. Most experimental studies, however, have focused on the apical membrane, despite the fact that ion transport across respiratory epithelia involves both cellular and paracellular pathways. In fact, the ion permeabilities of the basolateral membrane and paracellular pathway remain largely unknown. Here we use a biophysical model for water and ion transport to quantify ion permeabilities of all pathways (apical, basolateral, paracellular) in human nasal epithelia cultures using experimental (Ussing Chamber and microelectrode) data reported in the literature. We derive analytical formulas for the steady-state short-circuit current and membrane potential, which are for polarized epithelia the equivalent of the Goldman-Hodgkin-Katz equation for single isolated cells. These relations allow parameter estimation to be performed efficiently. By providing a method to quantify all the ion permeabilities of respiratory epithelia, the model may aid us in understanding the physiology that regulates normal airway surface hydration.

## INTRODUCTION

Normally, airway surface liquid (ASL) is ~98% water, 1% salt, and 1% proteins by weight, including the very high molecular weight mucins that determine the viscoelastic properties of the mucus layer. As demonstrated by recent studies (1), proper hydration is a requirement for efficient mucus clearance. Hydration of the airway surface is controlled by a balance between ion secretion and ion absorption. Most of the focus on the balance between secretion and absorption has been on the $Na^+$ and $Cl^-$ channels located in the apical membranes of airway epithelia. However, a complete understanding of ASL homeostasis requires a description of the full system, including ion transport across the basolateral membrane and the paracellular pathway. To this end, we developed a mathematical model of ion and water transport by the respiratory epithelium. The model is used to quantify the ion permeabilities of respiratory epithelia based on experimental data available in the literature.

Several mathematical models of epithelial ion transport have been reported (2–17). These models describe a range of epithelial types (respiratory, intestinal, corneal, kidney), from different animal species (human, rabbit, dog, mouse, frog), and different epithelial properties (leaky versus tight epithelia). Novotny and Jakobsson (5,6) published a seminal model for respiratory epithelia that was based on data from dog trachea. Their model was recently extended to human bronchial epithelia and used to investigate ASL pH regulation (9) and changes in cell volume that occurred after hypotonic challenges (8). Although these models include basolateral and paracellular ion transport, a systematic parameterization and validation of the models was not performed.

Our work extends that of Novotny and Jakobsson (5,6) in several significant ways. Our model includes apical $K^+$ and basolateral $Cl^-$ channels and distinguishes the paracellular permeabilities of anions and cations. Most importantly, the values of model parameters were estimated directly from experimental measurements of the transepithelial and intracellular bioelectric properties of human nasal epithelia (HNE) cultures measured in Ussing Chambers (18–20). To our knowledge, this is the first time that such a large dataset has been used to systematically estimate the ion permeabilities of human respiratory epithelia. Our findings provide a fuller description of ion transport in respiratory epithelia and may contribute to understanding of the normal hydrating process required for lung health.

## MATERIALS AND METHODS

### Model description

#### *Ions and transport pathways*

The model includes apical, basolateral, and cellular compartments separated by two membranes, the apical and the basolateral (Fig. 1 *A*). The apical membrane is permeable to $Na^+$, $K^+$, and $Cl^-$, while the basolateral membrane is permeable only to $K^+$ and $Cl^-$, as suggested by intracellular microelectrode experiments using nasal epithelial cell cultures (18–20).

*Submitted July 16, 2012, and accepted for publication December 4, 2012.*

*Correspondence: guilhermejmgarcia@gmail.com

Guilherme J. M. Garcia's present address is Biotechnology & Bioengineering Center, Medical College of Wisconsin, Milwaukee, WI, USA.

Editor: Jeffrey Fredberg.


0006-3495/13/02/0716/11 $2.00

http://dx.doi.org/10.1016/j.bpj.2012.12.040

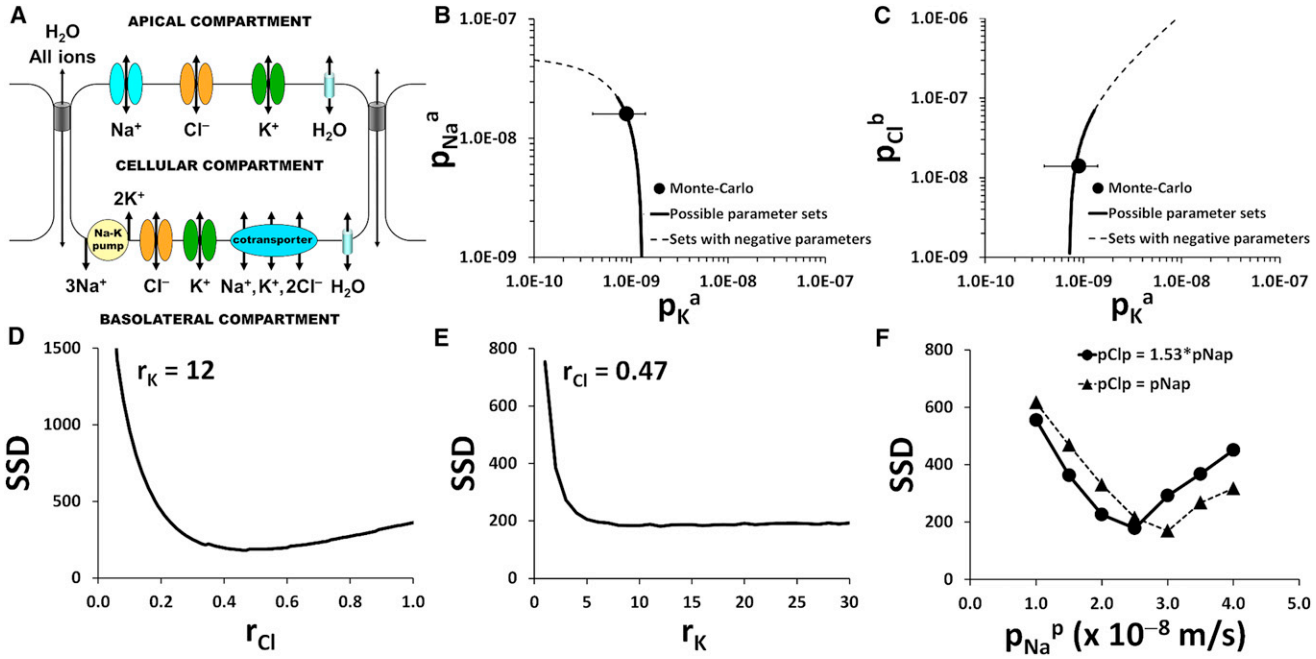


FIGURE 1 (*A*) Schematic diagram of the main pathways of ion and water transport in respiratory epithelia, all of which are included in the model. The paracellular pathway allows the diffusion of ions and water between the apical and basolateral compartments. The basolateral membrane expresses the Na-K pump, $Cl^-$ channels, $K^+$ channels, and the Na-K-2Cl cotransporter. The apical membrane expresses $Na^+$ channels, $Cl^-$ channels, and $K^+$ channels. Both basolateral and apical membranes are permeable to water. (*B–F*) Parameter fitting was accomplished using analytical expressions for the steady-state short-circuit current ($I_{SC}$) and membrane potential at short-circuit condition ($V_m$) to perform an efficient search of the parameter space. (*B* and *C*) Triplets of apical $Na^+$ permeability, apical $K^+$ permeability, and basolateral $Cl^-$ permeability $\{p^a_{Na}, p^a_K, p^b_{Cl}\}$ that reproduce the experimental $I_{SC}$ and $V_m$ as predicted by Eqs. 10 and 11 (*solid lines*). Some triplets $\{p^a_{Na}, p^a_K, p^b_{Cl}\}$ are associated with negative values of other ion permeabilities, which are physically unrealistic (*dashed lines*). The triplet $\{1.6, 0.09, 1.4\} \times 10^{-8}$ m/s obtained with a Monte Carlo method (see the Supporting Material) is shown for comparison (*symbols*). (*D* and *E*) By varying the ratios $r_K = p^b_K/p^a_K$ and $r_{Cl} = p^b_{Cl}/p^a_{Cl}$ and simulating various experimental conditions (see Table S3), the pair $\{r_K, r_{Cl}\}$ that minimized the score function SSD was identified for each set of paracellular permeabilities $\{p^p_{Na}, p^p_{Cl}\}$. (*F*) To estimate the $Na^+$ and $Cl^-$ paracellular permeabilities, these parameters were varied under the hypotheses $p^p_{Cl} = p^p_{Na}$ or $p^p_{Cl} = (D_{Cl}/D_{Na})p^p_{Na} = 1.53\,p^p_{Na}$. Simulations were run for various experimental conditions (see Table S3) and the best fits were obtained for $p^p_{Na} = 2.5–3.0 \times 10^{-8}$ m/s.

The Na-K pump and the Na-K-2Cl cotransporter (NKCC1) are localized to the basolateral membrane. Both membranes are permeable to water, but the water permeability of the apical membrane is greater than that of the basolateral membrane (21). The paracellular pathway connects the apical and basolateral compartments, allowing electrodiffusion of all ions and water between these two compartments directly, without crossing the cellular compartment (Fig. 1 *A*). The cellular compartment contains five chemical species ($H_2O$, $Na^+$, $K^+$, $Cl^-$, and IO), where all impermeable osmolytes (IO) are grouped as a single species. In addition to these species, the apical and basolateral compartments contain other ions found in KBR buffer ($Ca^{2+}$, $Mg^{2+}$, $HCO_3^-$, $HPO_4^{-2}$, $H_2PO_4^-$). The impermeant ions choline$^+$ and gluconate$^-$ are added to the apical and basolateral compartments to reproduce ion replacement studies (see Experimental Data below). It is assumed that all ions can cross the paracellular pathway and contribute to the paracellular electric current, but only $Na^+$, $K^+$, and $Cl^-$ can pass through ion channels in the cell membranes (Fig. 1 *A*).

### *Ion concentrations, ion activities, and osmolarity*

The concentration of ion $i$ in compartment $x$ ($[i]_x$, units of mM) is given by $[i]_x = N^x_i/H_x$, where $N^x_i$ (units of moles/m$^2$) is the number of moles of ion $i$ divided by the surface area of the cell culture and $H_x$ (units of m) is the compartment height. Each compartment is characterized by its liquid height, rather than its volume, because the surface area of the cell culture is constant. Throughout this article, subscripts or superscripts $a$, $b$, and $c$ denote the apical, basolateral, and cellular compartments, respectively.

To take into account the nonidealities of electrolyte solutions, the model is based on ion activities instead of ion concentrations. The activity of ion $i$ in compartment $x$ ($a_i^x$, units of mM) is related to its concentration via $a_i^x = \gamma_x[i]_x$, where the activity coefficient $\gamma_x$ is a nondimensional constant which depends on electrolyte chemical composition, concentration, and temperature (22). The activity coefficient of intracellular and extracellular solutions is not known for respiratory epithelia. Therefore, we assume $\gamma_a = \gamma_b = \gamma_c = \gamma_{NaCl}$, where $\gamma_{NaCl} = 0.76$ is the activity coefficient of a 300 mOsm/L NaCl solution at 310 K (22).

The osmolarity of compartment $x$ is given by $\mathrm{Osm}_x = \phi_x \sum [i]_x$, where $\phi_x$ is the osmotic coefficient of the solution in compartment $x$. For example, the osmolarity of the intracellular compartment is

$$\mathrm{Osm}_c = \phi_c\left([\mathrm{Na}]_c + [\mathrm{K}]_c + [\mathrm{Cl}]_c + [\mathrm{IO}]_c\right). \qquad (1)$$

Similarly to the activity coefficients, the precise values of the osmotic coefficients are unknown. Therefore, we assume $\phi_a = \phi_b = \phi_c = \phi_{NaCl}$, where $\phi_{NaCl} = 0.93$ is the osmotic coefficient of a 300 mOsm/L NaCl solution at 310 K (22).

### *Equations for ion transport*

The molar abundance per unit surface area of a given ion species in the cellular compartment is governed by an equation of the form

$$\frac{dN_i^c}{dt} = \sum J_i^m,$$

where $J_i^m$ (units of mols/s•m$^2$) is the flux per unit surface area of ion $i$ across the membrane $m$. Thus, the number of moles of sodium ($N^c_{Na}$), potassium ($N^c_K$), and chloride ($N^c_{Cl}$) in the cellular compartment are governed by the following equations:

$$\begin{aligned}\frac{d}{dt}N^c_{Na} &= J^a_{Na} + J^{PUMP}_{Na} + J^{CO}_{Na},\\ \frac{d}{dt}N^c_{K} &= J^a_{K} + J^b_{K} + J^{PUMP}_{K} + J^{CO}_{K},\\ \frac{d}{dt}N^c_{Cl} &= J^a_{Cl} + J^b_{Cl} + J^{CO}_{Cl}.\end{aligned} \quad (2)$$

The ion fluxes through the apical channels ($J^a_i$) and basolateral channels ($J^b_i$) are described below, while the fluxes through the Na-K pump ($J_i^{PUMP}$) and Na-K-2Cl cotransporter ($J_i^{CO}$) are described in the Supporting Material.

In contrast to permeable ions, impermeable osmolytes (IO) cannot cross cell membranes. Therefore, their molecular abundance ($N^c_{IO}$) is constant and determined by the initial ion concentrations, cell height, and osmolarity (Table 1) by assuming that all compartments are initially isotonic. Finally, the apical and basolateral compartments are assumed to be sufficiently large that their ion composition remains constant. We assume that apical and basolateral ion concentrations correspond to the KBR solution (115 mM NaCl, 25 mM $NaHCO_3$, 2.4 mM $K_2HPO_4$, 0.4 mM $KH_2PO_4$, 1.1 mM $CaCl_2$, 1.2 mM $MgCl_2$, 5.2 mM glucose) (see Table S1 in the Supporting Material).

### Equation for water transport

The equation for water transport is similar to the equations for ion transport. The number of moles of water in the cellular compartment per unit surface area of cell culture ($N^c_{H_2O}$, units of moles/m$^2$) is given by the definition of the molar volume of water, namely $N^c_{H_2O} = H_c/V_{H_2O}$, where $V_{H_2O} = 18.1 \times 10^{-6}$ m$^3$/mol is the molar volume of water. Substituting the latter expression into $dN^c_{H_2O}/dt = \sum_y J^m_{H_2O}$ and rearranging terms, we get $dH_c/dt = V_{H_2O}\sum_m J^m_{H_2O}$, where $J^m_{H_2O}$ is the water flux through the membrane $m$. The water flux is proportional to the osmotic gradient between compartments, so that changes in cell height ($H_c$) are described by

$$\frac{d}{dt}H_c = V_{H_2O}\left[p^a_{H_2O}(\mathrm{Osm}_c - \mathrm{Osm}_a) + p^b_{H_2O}(\mathrm{Osm}_c - \mathrm{Osm}_b)\right], \quad (3)$$

where $p^a_{H_2O}$ and $p^b_{H_2O}$ (units of m/s) are the water permeabilities of the apical and basolateral membranes, respectively.

Note that the term "water transport" in this article refers to water entering or leaving the cell, which only affects cell height and intracellular concentrations. Apical and basolateral solutions can be considered infinitely large in Ussing Chamber experiments and thus their composition remains constant. Also note that the geometric configuration of our three-compartment model (Fig. 1 *A*) is different from some previously published models (14,23). In these models, the intercellular space is considered a fourth compartment that is crucial for near-isotonic transepithelial fluid transport (14,23–25). Our basis for a three-compartment model is based on the following set of rationales:

1. The experimental observation that respiratory epithelia behave as perfect osmometers in osmotic challenge experiments (21);
2. There is no evidence (as of this writing) that the basolateral membrane can be separated into two functional regions (lateral versus serosal), and we are not aware of evidence that Na-K pumps are more concentrated along the intercellular space in respiratory epithelia, as has been suggested for other epithelial types (25);
3. Respiratory epithelia are structured as a monolayer, in contrast to other epithelial types where several layers of cells form long channels in the intercellular space; and
4. In the absence of contradicting evidence, we started from the simplest hypothesis.

Because our goal here is to use Ussing Chamber data to quantify the ion permeabilities, we leave transepithelial water transport to future studies, which will describe ASL volume regulation in thin-film conditions.

### Fluxes through ion channels and the paracellular pathway

The passive flux of ion $i$ across a membrane due to an electrochemical gradient is described by Goldman's constant field equation (26)

$$J_i^{y\to x} = \frac{p_i^m z_i \mu}{e^{z_i\mu} - 1}\left(a_i^y - a_i^x e^{z_i\mu}\right), \quad (4)$$

where $p_i^m$ is the membrane permeability (units of m/s), $z_i$ is the ion valence, $a_i^y$ is the activity of ion $i$ in compartment $y$ (units of mM), and $\mu = FV_m/RT$ is the nondimensional membrane potential, which depends on the membrane potential ($V_m$, units of $V$), the Faraday constant ($F$ = 96,485 C/mol), the gas constant ($R$ = 8.314 J/mol•K), and temperature ($T$ = 310 K). All passive fluxes through ion channels and the paracellular pathway were calculated using Eq. 4.

### Paracellular permeabilities

The paracellular pathway is permeable to all ions. To reduce the number of model parameters, only two paracellular permeabilities were considered independent parameters, namely the $Na^+$ paracellular permeability ($p^p_{Na}$) and the $Cl^-$ paracellular permeability ($p^p_{Cl}$). All other paracellular permeabilities were calculated from $p^p_i = (D_i/D_{Na})p^p_{Na}$ for cations and $p^p_i = (D_i/D_{Cl})p^p_{Cl}$ for anions, where $D_i$ is the diffusion coefficient of ion $i$ in water (see Table S2).

### Electric currents, membrane capacitance, and membrane potentials

Movement of ions across plasma membranes generates electric currents and membrane potentials. The electric current $I_i$ associated with an ion flux $J_i$ is given by $I_i = -Fz_iJ_i$, where $I_i$ is in units of A/m$^2$. Therefore, the currents through the apical membrane ($I^a$), basolateral membrane ($I^b$), and paracellular pathway ($I^p$) are given by

**TABLE 1 Steady-state properties of human nasal epithelium measured in Ussing Chambers with micro-electrodes compared to model simulations**

| | Experiment | Model |
|---|---|---|
| $a^c_{Na}$ (mM) | 23 ± 1 | 23.2 ± 0.3 |
| $a^c_K$ (mM) | 80 ± 5[a] | 80.2 ± 0.3 |
| $a^c_{Cl}$ (mM) | 44 ± 3 | 46.0 ± 0.6 |
| $V_a$ (mV) | −26 ± 3 | −24.4 ± 0.4 |
| $V_b$ (mV) | −38 ± 4 | −36.4 ± 0.4 |
| $V_t$ (mV) | −12 ± 2 | −12.0 ± 0.3 |
| $R_t$ (Ω/cm$^2$) | 338 ± 38 | 342 ± 7 |
| $fR_a$ | 0.47 ± 0.03 | 0.445 ± 0.006 |
| $I_{eq}$ ($\mu$A/cm$^2$) | 39 ± 5 | 35.0 ± 0.8 |
| $H_c$ ($\mu$m) | 29.3 ± 4.3 | 30.2 ± 0.3 |

The standard deviations in model simulations were estimated with a Monte Carlo algorithm (see the Supporting Material). The experimental data were taken from references (18,20,31,42,43).
[a]Dog tracheal epithelia.

$$
\begin{aligned}
I^a &= F\left(-J^a_{\mathrm{Na}} - J^a_{\mathrm{K}} + J^a_{\mathrm{Cl}}\right),\\
I^b &= F\left(J_{\mathrm{PUMP}} - J^b_{\mathrm{K}} + J^b_{\mathrm{Cl}}\right),\\
I^p &= F\Big[-J^p_{\mathrm{Na}} - J^p_{\mathrm{K}} - 2J^p_{\mathrm{Ca}} - 2J^p_{\mathrm{Mg}} - J^p_{\mathrm{choline}} + J^p_{\mathrm{Cl}}\\
&\quad + J^p_{\mathrm{HCO_3}} + J^p_{\mathrm{H_2PO_4}} + 2J^p_{\mathrm{HPO_4}} + J^p_{\mathrm{gluconate}}\Big]\\
&= F\Big[-J^p_{\mathrm{Na}} - J^p_{\mathrm{choline}} + J^p_{\mathrm{Cl}} + J^p_{\mathrm{gluconate}}\\
&\quad + \mu_t(9.752p^p_{\mathrm{Na}} + 13.809p^p_{\mathrm{Cl}})\Big].
\end{aligned}
\tag{5}
$$

Note that the flux through the Na-K-2Cl cotransporter does not contribute to the basolateral current, reflecting the electroneutral nature of the cotransporter.

To obtain a differential equation for the membrane potentials, we use the definition of a parallel plate capacitor, $q = CV$, where $q$ is the magnitude of the charge on one of the plates, $C$ is the plate capacitance, and $V$ is the voltage difference between plates. Noting that the charges in the apical and basolateral compartments are governed by the equations $dq_a/dt = (I^p - I^a + I_{\mathrm{ext}})$ and $dq_b/dt = -(I^p + I^b + I_{\mathrm{ext}})$, respectively, where $I_{\mathrm{ext}}$ is the electric current generated by an external voltage source (i.e., the electric circuitry in the Ussing Chamber), the apical and basolateral membrane potentials are determined, respectively, by

$$
\frac{dV_a}{dt} = \frac{1}{C_a}\left(I^p - I^a + I_{\mathrm{ext}}\right), \tag{6a}
$$

$$
\frac{dV_b}{dt} = -\frac{1}{C_b}\left(I^p + I^b + I_{\mathrm{ext}}\right). \tag{6b}
$$

The apical and basolateral membrane capacitances per unit surface area of respiratory epithelia cell cultures were reported as $C_a = 3.23 \pm 0.07$ $\mu$F/cm$^2$ and $C_b = 33.4 \pm 0.5$ $\mu$F/cm$^2$ (27). Note that these values are much higher than the capacitance per unit surface area of cell membrane, which is ~1 $\mu$F/cm$^2$ for all cell types (28).

### *Transepithelial resistance and apical fractional resistance*

By varying the current $I_{\mathrm{ext}}$ generated by the external electric circuitry, it is possible to manipulate the transepithelial potential ($V_t$). Varying the external current in the model provided a linear relation between $V_t$ and $I_{\mathrm{ext}}$. The transepithelial resistance ($R_t$) is defined as the slope of the voltage-current curve, namely

$$
R_t = \frac{\Delta V_t}{\Delta I_{\mathrm{ext}}}. \tag{7}
$$

To reproduce the experimental methods of Willumsen et al. (18,19), current pulses $\Delta I_{\mathrm{ext}} = 10$ $\mu$A of duration 0.5 s were used in our simulations to compute the transepithelial resistance.

Another parameter commonly measured experimentally is the apical fractional resistance ($fR_a$), which is defined as

$$
fR_a = \frac{R_a}{(R_a + R_b)} = -\frac{\Delta V_a}{\Delta V_t}, \tag{8}
$$

where $R_a = \Delta V_a/\Delta I^a$ and $R_b = \Delta V_b/\Delta I^b$ are the resistances of the apical and basolateral membranes, respectively. Here the symbol $\Delta$ denotes deflections in currents and potentials after changes in the external current ($\Delta I_{\mathrm{ext}}$).

## Derivation of steady-state solution for the short-circuit current and voltage

At steady state, intracellular concentrations are constant. Therefore, setting the derivatives in Eq. 2 to zero and eliminating $J_{\mathrm{PUMP}}$ and $J_{\mathrm{CO}}$, we find the relation

$$
4J^a_{\mathrm{Na}} + 6\left(J^a_{\mathrm{K}} + J^b_{\mathrm{K}}\right) - 5\left(J^a_{\mathrm{Cl}} + J^b_{\mathrm{Cl}}\right) = 0, \tag{9}
$$

where the coefficients 4, 6, and 5 follow from the stoichiometry of the Na-K pump and the Na-K-2Cl cotransporter (see the Supporting Material). By definition, under large-bath short-circuit conditions, the transepithelial potential is zero ($V_t = 0$, $V_a = V_b = V_m$) and the apical and basolateral baths have the same composition ($[i]_a = [i]_b$). Substituting the expression for ion fluxes (Eq. 4 into Eq. 9 and solving for $V_m$), we find

$$
V_m = \frac{RT}{F} ln\left(\frac{4p^a_{\mathrm{Na}}[\mathrm{Na}]_b + 6\left(p^a_{\mathrm{K}} + p^b_{\mathrm{K}}\right)[\mathrm{K}]_b + 5\left(p^a_{\mathrm{Cl}} + p^b_{\mathrm{Cl}}\right)[\mathrm{Cl}]_c}{4p^a_{\mathrm{Na}}[\mathrm{Na}]_c + 6\left(p^a_{\mathrm{K}} + p^b_{\mathrm{K}}\right)[\mathrm{K}]_c + 5\left(p^a_{\mathrm{Cl}} + p^b_{\mathrm{Cl}}\right)[\mathrm{Cl}]_b}\right). \tag{10}
$$

Note that, strictly speaking, this equation should be written in terms of ion activities, and that Eq. 10 represents the case $\gamma_a = \gamma_b = \gamma_c$. Using the definition of the apical current (Eq. 5), the analytical solution for the short-circuit current at steady state is

$$
I_{SC} = F\mu_m \frac{(C_2 e^{\mu_m} - C_1)}{(e^{\mu_m} - 1)}, \tag{11}
$$

where $C_1 = p^a_{\mathrm{Na}}a^a_{\mathrm{Na}} + p^a_{\mathrm{K}}a^a_{\mathrm{K}} + p^a_{\mathrm{Cl}}a^c_{\mathrm{Cl}}$, $C_2 = p^a_{\mathrm{Na}}a^c_{\mathrm{Na}} + p^a_{\mathrm{K}}a^c_{\mathrm{K}} + p^a_{\mathrm{Cl}}a^a_{\mathrm{Cl}}$, and $\mu_m = FV_m/RT$.

Defining $K = I_{SC}\dfrac{(e^{\mu_m} - 1)}{F\mu_m}$, we find that Eqs. 10 and 11 can be used to express the apical $Na^+$ permeability ($p^a{}_{\mathrm{Na}}$) and basolateral $Cl^-$ permeability ($p^b{}_{\mathrm{Cl}}$) as a function of the apical $K^+$ permeability ($p^a{}_{\mathrm{K}}$), namely

$$
\begin{aligned}
p^a_{\mathrm{Na}} &= \frac{5(1 + r_{\mathrm{Cl}})K + p^a_{\mathrm{K}}\xi_{\mathrm{K}}(1 + 6r_{\mathrm{K}} - 5r_{\mathrm{Cl}})}{\xi_{\mathrm{Na}}(1 + 5r_{\mathrm{Cl}})},\\
p^b_{\mathrm{Cl}} &= \frac{-4K - p^a_{\mathrm{K}}\xi_{\mathrm{K}}(2 + 6r_{\mathrm{K}})}{\xi_{\mathrm{Cl}}(5 + r^{-1}_{\mathrm{Cl}})},
\end{aligned}
\tag{12}
$$

where $r_{\mathrm{Cl}} = p^b{}_{\mathrm{Cl}}/p^a{}_{\mathrm{Cl}}$ and $r_{\mathrm{K}} = p^b{}_{\mathrm{K}}/p^a{}_{\mathrm{K}}$ are basolateral-to-apical permeability ratios and $\xi_{\mathrm{Na}} = e^{\mu_m}a^c_{\mathrm{Na}} - a^a_{\mathrm{Na}}$, $\xi_{\mathrm{K}} = e^{\mu_m}a^c_{\mathrm{K}} - a^a_{\mathrm{K}}$, and $\xi_{\mathrm{Cl}} = e^{\mu_m}a^a_{\mathrm{Cl}} - a^c_{\mathrm{Cl}}$ are the electrochemical gradients.

## Experimental data

The experimental data used to fit model parameters were collected from Willumsen and co-workers (18–20) and represent the most complete dataset available for the bioelectric properties of primary cultures of human respiratory epithelia. Using the perfused Ussing Chamber technique and ion-selective intracellular microelectrodes, these authors reported the results of various pharmacological interventions on a number of variables (ion activities, membrane potentials, epithelial resistance, apical fractional resistance, and equivalent short-circuit current).

We found that steady-state properties alone (Table 1) were not sufficient to constrain model parameters. Therefore, the experimental dataset used to fit the model also included the effects of amiloride ($Na^+$ channel blocker), bumetanide (Na-K-2Cl cotransporter blocker), reduction of basolateral $Na^+$ to 3 mM, and reduction of basolateral $Cl^-$ to 3 mM (see Table S3). To test whether the model was predictive of epithelial behavior, model predictions were compared to experimental data for the effects of ouabain (Na-K pump inhibitor), reduction of apical $Na^+$ to 3 mM, and reduction of apical $Cl^-$ to 3 mM. That is, a subset of the experimental data available was used to train the model, while another subset was used to validate the model (see Table S3). The simulations assumed that each inhibitor completely blocked its

target transport pathway (i.e., amiloride: $p^{a}_{Na} = 0$; bumetanide: $J^{max}_{CO} = 0$; ouabain: $J^{max}_{PUMP} = 0$).

## Parameter estimation

All experimental data points, including all variables and all time points, were written as a matrix $\mathbf{Y}^{EXP}$, where the rows of $\mathbf{Y}^{EXP}$ represent different time points and the columns of $\mathbf{Y}^{EXP}$ are the experimental readouts. The score function was defined as

$$SSD = \sum_{t,\,v} \frac{\left[Y^{EXP}_{t,v} - Y^{MODEL}_{t,v}\right]^2}{2\left[\sigma^{EXP}_{t,v}\right]^2}, \qquad (13)$$

where SSD is the sum of square differences between experimental data and model predictions, $\mathbf{Y}^{MODEL}$. The standard deviation in the experimental data $\boldsymbol{\sigma}^{EXP}$ was used to normalize the squared differences, so that parameters with different units and different magnitudes contribute equally to SSD.

The model has a total of 51 parameters (see the Supporting Material). Some parameters were held constant, while others were varied to fit the experimental data. The 42 parameters held constant were the ion composition of the bathing solution, activity coefficients, osmotic coefficients, membrane capacitances, water permeabilities, and the kinetics of the Na-K pump and Na-K-2Cl cotransporter, whose values were obtained from the literature (see Table S1). The nine parameters estimated from the data were the apical, basolateral, and paracellular ion permeabilities, the maximum flux through the Na-K pump, and the maximum flux through the Na-K-2Cl cotransporter (Table 2).

The algorithm used for parameter fitting can be summarized as follows: The analytical solution for the short-circuit current ($I_{SC}$) and membrane potential ($V_m$) provides parameter sets that are consistent with steady-state values of $I_{SC}$ and $V_m$, thus allowing an efficient search of the parameter space. First, we assumed that the paracellular permeabilities ($p^{p}_{Na}$, $p^{p}_{Cl}$) and permeability ratios ($r_K$, $r_{Cl}$) were known. Parameter sets that reproduce $I_{SC}$ and $V_m$ were obtained from the expressions in Eq. 12. Second, the permeability ratios were varied in the ranges $r_K \in [1,30]$ and $r_{Cl} \in [0.01, 1.0]$ and simulations were run to reproduce the experimental maneuvers (see Table S3). The pair $\{r_K, r_{Cl}\}$ that minimized the score function SSD was selected as the best fit. Third, to estimate the $Na^+$ and $Cl^-$ paracellular permeabilities, the steps above were repeated for several pairs $\{p^{p}_{Na}, p^{p}_{Cl}\}$ under the hypotheses $p^{p}_{Cl} = p^{p}_{Na}$ or $p^{p}_{Cl} = (D_{Cl}/D_{Na})p^{p}_{Na} = 1.53\ p^{p}_{Na}$ and the minimum SSD value was searched for. A more detailed description of this parameter fitting strategy can be found in the Supporting Material. To estimate error bars and prediction bands, a Monte Carlo method was used (see the Supporting Material).

**TABLE 2 Ion permeabilities of human nasal epithelia estimated by fitting model parameters to reproduce Ussing Chamber and microelectrode experimental data**

| | $p^{p}_{Cl} = p^{p}_{Na}$ | $p^{p}_{Cl} = 1.53\ p^{p}_{Na}$ |
|---|---|---|
| $p^{a}_{Na}$ ($\times 10^{-8}$ m/s) | 1.66 | 1.70 |
| $p^{a}_{K}$ ($\times 10^{-8}$ m/s) | 0.26 | 0.26 |
| $p^{a}_{Cl}$ ($\times 10^{-8}$ m/s) | 4.3 | 4.0 |
| $p^{b}_{K}$ ($\times 10^{-8}$ m/s) | 7.9 | 7.8 |
| $p^{b}_{Cl}$ ($\times 10^{-8}$ m/s) | 1.8 | 1.7 |
| $p^{p}_{Na}$ ($\times 10^{-8}$ m/s) | 3.0 | 2.5 |
| $p^{p}_{Cl}$ ($\times 10^{-8}$ m/s) | 3.0 | 3.8 |
| $J^{max}_{PUMP}$ ($\times 10^{-6}$ mol/m$^2$.s) | 3.8 | 3.8 |
| $J^{max}_{CO}$ ($\times 10^{-6}$ mol/m$^2$.s) | 3.9 | 3.6 |
| SSD | 169.2 | 178.6 |

The training dataset included: steady state (Table 1), amiloride (Fig. 2 *A*), bumetanide (Fig. 2 *B*), reduction of basolateral [$Na^+$] to 3 mM (Fig. 2 *C*), and reduction of basolateral [$Cl^-$] to 3 mM (Fig. 2 *D*). Results are shown for two assumptions regarding the paracellular permeabilities ($p^p$), namely, $p^{p}_{Cl} = p^{p}_{Na}$ and $p^{p}_{Cl} = 1.53\ p^{p}_{Na}$.

# RESULTS

## Analysis of model performance

The model successfully captured the steady-state bioelectric properties of nasal epithelia, including intracellular ion composition, membrane potentials, epithelial resistance, equivalent short-circuit current, and cell height (Table 1).

### *Inhibition of apical $Na^+$ permeability*

The addition of amiloride blocks the sodium channel ENaC and produces a drop in short-circuit current, hyperpolarization of the apical membrane, reduction in magnitude of the transepithelial potential, and an increase in the apical fractional resistance (Fig. 2 *A*). Model simulations were in good agreement with these experimental observations. However, one difference between model results and experiments is noteworthy. Experimentally, intracellular $Na^+$ remained nearly constant after amiloride addition, while the model predicted a drop in $a^{c}_{Na}$ (Fig. 2 *A*). Willumsen and Boucher (19) noted that this "surprising response" was inconsistent with the drop in intracellular sodium after amiloride treatment reported for other epithelial types (29). This "surprising response" of respiratory epithelia probably reflects the existence of other $Na^+$ transport pathways that were not included in the model. For example, it is known that amiloride-sensitive $Na^+$-$H^+$ exchangers are expressed in the basolateral membrane of respiratory epithelia (30). Thus, a possible explanation for the nearly-constant $a^{c}_{Na}$ observed experimentally is that amiloride blocks $Na^+$ exit through $Na^+$-$H^+$ exchangers, allowing $Na^+$ entry through the Na-K-2Cl cotransporter to increase the intracellular $Na^+$ concentration. This effect will be tested in future versions of the model.

### *Inhibition of the Na-K-2Cl cotransporter*

The addition of bumetanide (which blocks the Na-K-2Cl cotransporter) to the basolateral compartment causes a slow decrease in intracellular chloride and a slow increase in intracellular sodium (Fig. 2 *B*) (18). These changes in intracellular ion activities are accompanied by cell shrinkage and only minor, if any, changes in other bioelectric properties (18,19). These features were reproduced by the model, except that intracellular $Na^+$ did not increase, but rather remained constant (Fig. 2 *B*). Willumsen and Boucher (19) reasoned that cell shrinkage was associated with loss of $K^+$ and $Cl^-$ ions, so that intracellular $Na^+$ would concentrate during cell shrinkage. Our computational results reveal proportional losses of both $Na^+$ and $K^+$ during cell shrinkage, thus keeping the intracellular concentrations of these ions constant. However, if proportional losses of $Na^+$ and $K^+$ after bumetanide are possible, what explains the increased intracellular $Na^+$ (Fig. 2 *B*)?

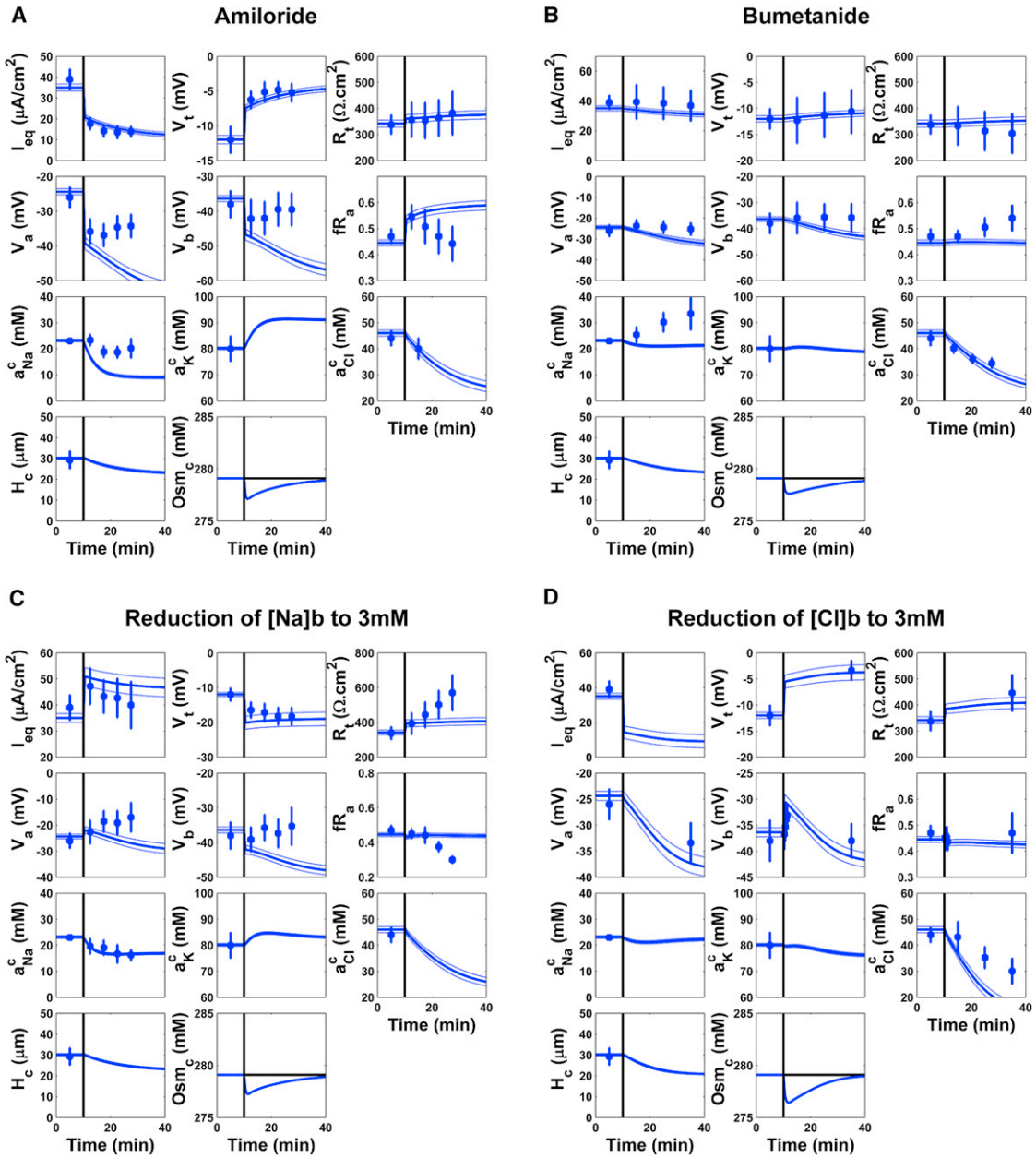


FIGURE 2 Model results (*solid lines*) are compared with experimental data (*symbols*) from open-circuit Ussing Chamber experiments using cultures of human nasal epithelium (HNE) (18,19). (*Dashed lines*) Prediction bands (two SDs around ensemble average) obtained with a Monte Carlo method (see the Supporting Material). Addition of drugs or changes in buffer solution occurred at 10 min (see *vertical line*). (*A*) Effect of inhibition of apical $Na^+$ channels with amiloride. (*B*) Inhibition of the Na-K-2Cl cotransporter with bumetanide. (*C*) Reduction of basolateral $Na^+$ from 140 mM to 3 mM by choline$^+$ replacement. (*D*) Reduction of basolateral $Cl^-$ from 119.6 mM to 3 mM by gluconate$^-$ replacement.

One interpretation is that bumetanide-induced cell shrinkage deactivates the Na-K pump, thus increasing $a^c_{Na}$. This interpretation is based on the experimental observation that cell shrinkage induced by hypertonic challenge also increases $a^c_{Na}$ in human nasal epithelium (31). This hypertonic-challenge-induced increase in intracellular $Na^+$ is accompanied by a decrease in the equivalent short-circuit current, which suggests reduced transepithelial $Na^+$ transport and downregulation of the Na-K pump (31).

### *Reduction of basolateral $Na^+$ to 3 mM*

Reduction of basolateral sodium from 140 mM to 3 mM did not have acute effects on the membrane potentials and epithelial resistances in Ussing Chamber experiments, leading Willumsen and Boucher (19) to conclude that the basolateral $Na^+$ permeability of nasal epithelia is low. Prolonged exposure to low basolateral $Na^+$ caused a drop in $a^c_{Na}$ due to $Na^+$ loss through the Na-K-2Cl cotransporter. This decrease in intracellular $Na^+$ caused depolarization

of the apical membrane, hyperpolarization of $V_t$, an increase in $R_t$, and a decrease in $fR_a$ (Fig. 2 *C*). The increase in $R_t$ accompanied by a drop in $fR_a$ was interpreted by Willumsen and Boucher (19) as inhibition of a basolateral ion conductance, possibly basolateral $K^+$ channels. Model simulations reproduced most of the effects of low basolateral $Na^+$, except that the rate of increase in $R_t$ and the rate of decrease in $fR_a$ were smaller in the model than in the experiments (Fig. 2 *C*). Thus, our simulations are consistent with the interpretation by Willumsen and Boucher (19) that cells respond to low basolateral $Na^+$ by decreasing the basolateral $K^+$ permeability, possibly by also reducing the flux through the Na-K pump to prevent intracellular $Na^+$ from falling to even lower levels.

#### *Reduction of basolateral $Cl^-$ to 3 mM*

Chloride replacement with gluconate$^-$ in the basolateral solution caused a decrease in intracellular $Cl^-$ that was faster in the model than in the experimental data (Fig. 2 *D*). The model successfully predicted that this maneuver leads to hyperpolarization of the apical membrane, depolarization of the transepithelial potential, and an increase in epithelial resistance (Fig. 2 *D*).

### Estimated ion permeabilities

To estimate the ion permeabilities, we first assumed that the paracellular permeabilities and permeability ratios were known. Initial guesses for these parameters ($p^p_{Na} = 2.8 \times 10^{-8}$ m/s, $p^p_{Cl} = 3.0 \times 10^{-8}$ m/s, $r_K = 91.1$, and $r_{Cl} = 0.35$) were derived from a Monte Carlo parameter fitting strategy (see the Supporting Material). Using Eqs. 2 and 12, parameter sets that reproduce $I_{SC}$ and $V_m$ were obtained and those sets that contained any negative values were discarded (Fig. 1, *B* and *C*).

Next, the permeability ratios $\{r_K, r_{Cl}\}$ were varied and simulations were run to reproduce the experimental maneuvers (see Table S3). The pair $\{r_K, r_{Cl}\}$ that minimized the score function SSD was selected as the best fit (Fig. 1, *D* and *E*). Finally, to estimate the paracellular permeabilities, the steps above were repeated for several pairs $\{p^p_{Na}, p^p_{Cl}\}$ under the hypotheses $p^p_{Cl} = p^p_{Na}$ or $p^p_{Cl} = (D_{Cl}/D_{Na})p^p_{Na} = 1.53\ p^p_{Na}$, and the minimum SSD value was searched for. The best fits were obtained for $p^p_{Na} = 2.5$–$3.0 \times 10^{-8}$ m/s (Fig. 1 *F*). The ion permeabilities thus obtained are listed in Table 2. As discussed below, our estimates of ion permeabilities are consistent with previous literature.

Willumsen, Boucher, and co-worker (19,20,32) estimated $p^a_{Cl}$ in the range 3.6–7.2 $\times 10^{-8}$ m/s and $p^a_{Na}$ in the range 1.6–2.8 $\times 10^{-8}$ m/s for human nasal epithelia. Despite the fact that their model assumed that the apical membrane under resting conditions is impermeable to $K^+$ ($p^a_K = 0$), our estimates of $p^a_{Cl} = 4.3 \times 10^{-8}$ m/s and $p^a_{Na} = 1.7 \times 10^{-8}$ m/s (Table 2) are in good agreement with their estimates and support their hypothesis of a low basal apical $K^+$ permeability. To the best of our knowledge, the expression levels of apical $K^+$ channels have not been quantified in human nasal epithelia, although previous studies suggested that $p^a_K$ is smaller than $p^a_{Cl}$ (33). The scarcity of data on apical $K^+$ channels in human respiratory epithelia is largely due to the secondary role played by this permeability. In nasal epithelia, the model suggests that basal $p^a_K$ is six times smaller than $p^a_{Na}$ and 17 times smaller than $p^a_{Cl}$. Note, however, that it was recently demonstrated that apical voltage-dependent $K^+$ channels are critical for ASL hydration in human bronchial epithelia (34).

Although the basolateral ion permeabilities had never been quantified, based on the magnitude of shifts in $fR_a$ after ion replacement studies, Willumsen et al. (18,19) predicted that the basolateral conductance was dominated by $K^+$ with a smaller contribution of $Cl^-$. This prediction was confirmed by our model, where the ratio of $K^+$ to $Cl^-$ basolateral permeabilities is approximately four in human nasal epithelia (Table 2).

The paracellular pathway is perhaps the least studied and least understood ion transport pathway in airway epithelia. In fact, some researchers have concluded that this pathway is anion-selective (35), while others reported that it is cation-selective (36). Previous mathematical models of respiratory epithelia assumed identical paracellular permeabilities for all ions (5) or assumed only paracellular transport of $Na^+$ and $Cl^-$, but no paracellular transport of $K^+$ and other ions in the bathing solution (8). Here, we assumed that the paracellular pathway is permeable to all ions in the KBR buffer (Fig. 1 *A*) and that their relative paracellular permeabilities follow the same ratio as their ionic diffusivities in water (see Table S2). The parameters estimated suggest that paracellular permeabilities of $Na^+$ and $Cl^-$ are about the same in human nasal epithelial cultures (Table 2).

### Model validation

To test the validity of the model and estimated parameters (Table 2), the model was used to predict the response of the system to various experimental perturbations.

#### *Inhibition of the Na-K pump*

Inhibition of the Na-K pump by the addition of ouabain resulted in the dissipation of ionic gradients and, consequently, depolarization of the membrane potentials and abolition of $I_{eq}$ (Fig. 3 *A*). Model simulations reproduced the experimental data, including the observation that epithelial resistance remains nearly constant during the 50 min after ouabain addition (Fig. 3 *A*).

#### *Reduction of apical $Na^+$ to 3 mM*

Partial replacement of $Na^+$ by impermeant choline$^+$ in the apical solution caused a sharp fall in intracellular $Na^+$, followed by hyperpolarization of the apical membrane,

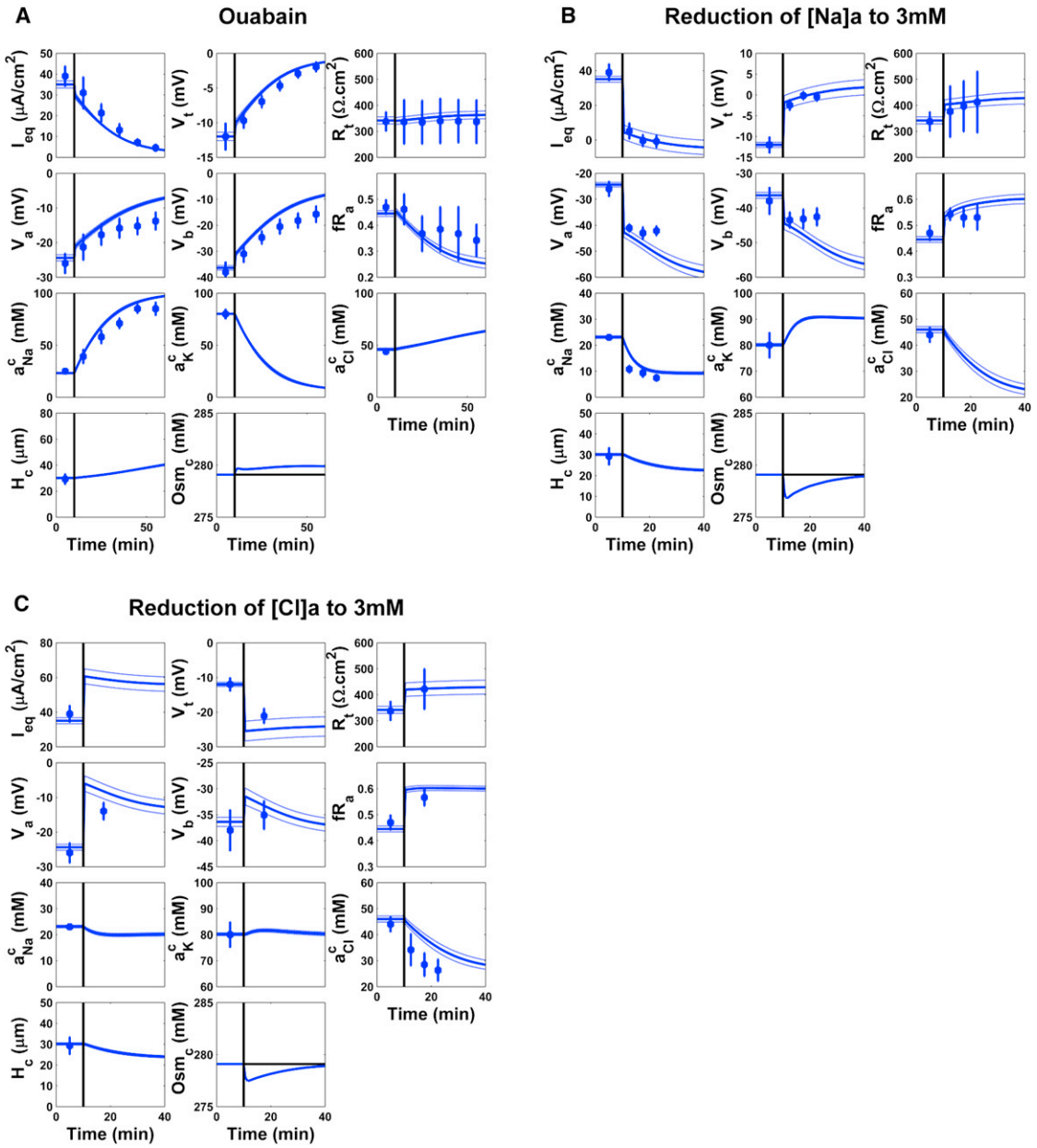


FIGURE 3 Model predictions (*solid lines*) are compared with experimental data (*symbols*) from open-circuit Ussing Chamber experiments using cultures of human nasal epithelium (HNE) (18,19). (*Dashed lines*) Prediction bands (two SDs around ensemble average) obtained with a Monte Carlo method (see the Supporting Material). Addition of drug or changes in buffer solution occurred at 10 min (see *vertical line*). (*A*) Inhibition of the Na-K pump with ouabain. (*B*) Reduction of apical $Na^+$ from 140 mM to 3 mM by choline$^+$ replacement (18,19). (*C*) Reduction of apical $Cl^-$ from 119.6 mM to 3 mM by gluconate$^-$ replacement (18,19).

depolarization of the transepithelial potential, increased epithelial resistance, and reduced equivalent short-circuit current (Fig. 3 *B*). Model simulations reproduced these effects very well, including a drop in intracellular $Na^+$ and an increase in $fR_a$ (Fig. 3 *B*). Because the effects of apical $Na^+$ replacement by an impermeant cation are similar to the effects of amiloride, model predictions for $Na^+$ replacement are similar to its predictions for amiloride (compare Figs. 2 *A* and 3 *B*). This similarity between $Na^+$ replacement and amiloride treatment is also seen in the experimental data.

### *Reduction of apical $Cl^-$ to 3 mM*

Simulations of partial $Cl^-$ replacement with impermeant gluconate$^-$ in the apical solution reproduced the drop in intracellular $Cl^-$, depolarization of the apical membrane, hyperpolarization of the transepithelial potential, increase in epithelial resistance, and increase in the fractional

resistance of the apical membrane observed experimentally (Fig. 3 *C*).

## DISCUSSION

The main pathways for ion transport in human respiratory epithelia have been identified, but their relative contributions to epithelial behaviors under a variety of conditions have not been quantified. In particular, the basolateral and paracellular ion permeabilities of human nasal epithelia have not been estimated systematically. To elucidate and quantify these ion permeabilities, we developed a mathematical model for ion/water transport in the human respiratory epithelium. Many mathematical models of epithelial electrophysiology exist, but most models were developed for different epithelial types or nonhuman species (2–16).

Recently, two models for human respiratory epithelia were reported. These studies focused on pH regulation (9) and the regulation of cell volume following a hypotonic challenge (8). In contrast, our study was aimed at quantifying the expression levels of the principal ion transport pathways in nasal epithelia by systematically investigating the parameter space of the mathematical model. The dataset used to parameterize the model consisted of a large number of experimental measurements of both transepithelial and intracellular HNE parameters, which represents the most complete characterization of primary cultures of human respiratory epithelium currently available in the literature. Model simulations were generally in good agreement with the data and, when quantitative agreement was not achieved, the model produced qualitatively correct behavior.

Some limitations of our work should be noted: Our model does not account for all transporters and exchangers experimentally observed in respiratory epithelia; it accounts only for the components that are believed to play a central role in regulating ASL volume. Components that are not present in our model include Na-H exchangers, Cl-$HCO_3$ exchangers, Na-$HCO_3$ cotransporters (30,37–39), and the bicarbonate conductance of CFTR (40), which are all involved in pH regulation (9). Therefore, readers should note that our analytical equations for short-circuit current and membrane potential (Eqs. 10 and 11) are valid only when the membrane permeabilities for $Na^+$, $K^+$, and $Cl^-$ dominate over other ionic species. For respiratory epithelia, this is a good approximation and thus we opted to simplify the analyses, allowing a full description of the dynamic behavior of the system. Understanding the behavior of this simplified model will be helpful for the development of more complex models. We are, as of this writing, working on expanding the model to investigate how addition of $H^+$ and $HCO_3^-$ transport will affect the model's behavior.

Another potential limitation of the results reported here is that regulation of ion channels by intracellular signals was not incorporated because this regulation has not been characterized in an integrated fashion. Therefore, each experimental maneuver was simulated by changing only its primary target (e.g., reduction of $[Na]_b$ to 3 mM) while possible secondary effects due to intracellular signaling (e.g., reduction of $[Na]_b$ may inhibit $p^b_K$; see Results) were not simulated. Finally, experimental measurements of intracellular $K^+$ activity in human nasal epithelia could not be found. Thus, the steady-state value (80 mM) reported for canine tracheal epithelia was adopted. Considering these potential sources of error, the agreement between the model and experimental data is considered very good.

Model estimates of ion permeabilities are in good agreement with what is known about human nasal epithelia. More specifically, the model reproduced the experimental observations that

1. Apical $Cl^-$ permeability is larger than apical $Na^+$ permeability ($p^a_{Cl} > p^a_{Na}$) (20,32);
2. The apical $K^+$ permeability under basal conditions is relatively small (18); and
3. The basolateral $K^+$ permeability dominates the basolateral conductance (41) (Table 2).

The fact that these predictions are in agreement with the experimental literature gives us confidence in the model and the estimated parameter values. Another result that brings credibility to the model is the fact that it can be used to predict epithelial behavior for experimental conditions that were not used to train model parameters (Fig. 3).

A, to our knowledge, novel contribution of this article is the analytical formulae for short-circuit current and membrane potential at short-circuit conditions (Eqs. 10 and 11). These equations are useful to investigate the relationship between the expression levels of ion channels and the bioelectric measurements performed in Ussing chamber experiments. Here, we used these steady-state solutions to establish constraints between model parameters (Eq. 12), which allowed for an effective search of the parameter space. The analytical expressions for $I_{SC}$ and $V_m$ were consistent with the numerical solution.

Our results are qualitatively consistent with previous mathematical models of ion transport in polarized epithelia (2–9). For example, Levin et al. (7) found that amiloride causes a drop in $I_{SC}$, a fall in $V_t$ associated with increases in both $V_a$ and $V_b$, a fall in intracellular $Na^+$, and an increase in intracellular $K^+$, as we also obtained (Fig. 2 *A*). Willumsen and Boucher (20) used an equivalent circuit model to estimate the apical $Na^+$ and $Cl^-$ permeabilities of human nasal epithelia (20). Our estimates of $p^a_{Na}$ and $p^a_{Cl}$ are in good agreement with their conclusion that apical $Cl^-$ permeability is 2–3 times larger than apical $Na^+$ permeability.

In contrast, Novotny and Jakobsson assumed that $p^a_{Cl}$ and $p^a_{Na}$ are about the same, while Horisberger (17) assumed that $p^a_{Cl}$ is smaller than $p^a_{Na}$ (see Table S5). A comparison

between the ion permeabilities estimated in this study with other models in the literature reveals other important differences (see Table S5). For example, Horisberger (17) assumed that the basolateral $Cl^-$ permeability is fivefold larger than its apical counterpart, while we estimated that $p^b_{Cl}$ is actually ~1/2 of $p^a_{Cl}$. Warren et al. (8) assumed that the paracellular shunt is sixfold more permeable to $Na^+$ than to $Cl^-$, while we estimated that $p^p_{Na}$ and $p^p_{Cl}$ are about the same. These differences in assumed ion permeabilities suggest that, in some circumstances, the behavior of each of these models may be different quantitatively, if not qualitatively, from the actual epithelial behavior observed experimentally.

In summary, we presented a mathematical model of ion/water transport in the human respiratory epithelium. The model is predictive of the bioelectric behavior of nasal epithelia in a range of experimental conditions. In addition to confirming previous estimates of apical $Na^+$ permeability and apical $Cl^-$ permeability of human nasal epithelia, the model predicts the basolateral and paracellular permeabilities. By providing a fuller view of ion transport in respiratory epithelia, this mathematical model may be used to interpret experimental data, plan new ion transport experiments, and hopefully assist in the development of new therapies to treat pulmonary diseases.

## SUPPORTING MATERIAL

Supporting equations, five tables, three figures, and references (44–52) are available at http://www.biophysj.org/biophysj/supplemental/S0006-3495(12)05156-9.

We thank Dr. Eric Jakobsson and Dr. Cibele Falkenberg (University of Illinois at Urbana-Champaign) for insightful discussions on modeling the bioelectric properties of respiratory epithelia. We are also grateful to Dr. Maryse Picher, Dr. Brian Button, and Dr. Rob Tarran (Cystic Fibrosis Center, University of North Carolina at Chapel Hill) for discussions on ion transport in respiratory epithelia.

Funding was provided by the National Institutes of Health grants No. 5P01HL034322-24 and No. R01HL077546. G.J.M.G. also acknowledges funding by the Conselho Nacional de Desenvolvimento Científico e Tecnológico (the Brazilian Science Agency).

## REFERENCES

1. Boucher, R. C. 2007. Cystic fibrosis: a disease of vulnerability to airway surface dehydration. *Trends Mol. Med.* 13:231–240.
2. Lew, V. L., H. G. Ferreira, and T. Moura. 1979. The behavior of transporting epithelial cells. I. Computer analysis of a basic model. *Proc. R. Soc. Lond. B Biol. Sci.* 206:53–83.
3. Hartmann, T., and A. S. Verkman. 1990. Model of ion transport regulation in chloride-secreting airway epithelial cells. Integrated description of electrical, chemical, and fluorescence measurements. *Biophys. J.* 58:391–401.
4. Duszyk, M., and A. S. French. 1991. An analytical model of ionic movements in airway epithelial cells. *J. Theor. Biol.* 151:231–247.
5. Novotny, J. A., and E. Jakobsson. 1996. Computational studies of ion-water flux coupling in the airway epithelium. I. Construction of model. *Am. J. Physiol.* 270:C1751–C1763.
6. Novotny, J. A., and E. Jakobsson. 1996. Computational studies of ion-water flux coupling in the airway epithelium. II. Role of specific transport mechanisms. *Am. J. Physiol.* 270:C1764–C1772.
7. Levin, M. H., J. K. Kim, …, A. S. Verkman. 2006. Potential difference measurements of ocular surface $Na^+$ absorption analyzed using an electrokinetic model. *Invest. Ophthalmol. Vis. Sci.* 47:306–316.
8. Warren, N. J., M. H. Tawhai, and E. J. Crampin. 2009. A mathematical model of calcium-induced fluid secretion in airway epithelium. *J. Theor. Biol.* 259:837–849.
9. Falkenberg, C. V., and E. Jakobsson. 2010. A biophysical model for integration of electrical, osmotic, and pH regulation in the human bronchial epithelium. *Biophys. J.* 98:1476–1485.
10. Quraishi, I. H., and R. M. Raphael. 2007. Computational model of vectorial potassium transport by cochlear marginal cells and vestibular dark cells. *Am. J. Physiol. Cell Physiol.* 292:C591–C602.
11. Zhu, H., and A. Chauhan. 2007. Tear dynamics model. *Curr. Eye Res.* 32:177–197.
12. Schultz, S. G. 1998. A century of (epithelial) transport physiology: from vitalism to molecular cloning. *Am. J. Physiol.* 274:C13–C23.
13. Spring, K. R. 1999. Epithelial fluid transport—a century of investigation. *News Physiol. Sci.* 14:92–98.
14. Larsen, E. H., N. J. Willumsen, …, J. N. Sørensen. 2009. The lateral intercellular space as osmotic coupling compartment in isotonic transport. *Acta Physiol. (Oxf.).* 195:171–186.
15. Fischbarg, J., and F. P. Diecke. 2005. A mathematical model of electrolyte and fluid transport across corneal endothelium. *J. Membr. Biol.* 203:41–56.
16. Fischbarg, J., F. P. Diecke, …, A. Rubashkin. 2006. The role of the tight junction in paracellular fluid transport across corneal endothelium. Electro-osmosis as a driving force. *J. Membr. Biol.* 210:117–130.
17. Horisberger, J. D. 2003. ENaC-CFTR interactions: the role of electrical coupling of ion fluxes explored in an epithelial cell model. *Pflugers Arch.* 445:522–528.
18. Willumsen, N. J., C. W. Davis, and R. C. Boucher. 1989. Intracellular $Cl^-$ activity and cellular $Cl^-$ pathways in cultured human airway epithelium. *Am. J. Physiol.* 256:C1033–C1044.
19. Willumsen, N. J., and R. C. Boucher. 1991. Sodium transport and intracellular sodium activity in cultured human nasal epithelium. *Am. J. Physiol.* 261:C319–C331.
20. Willumsen, N. J., and R. C. Boucher. 1989. Shunt resistance and ion permeabilities in normal and cystic fibrosis airway epithelia. *Am. J. Physiol.* 256:C1054–C1063.
21. Matsui, H., C. W. Davis, …, R. C. Boucher. 2000. Osmotic water permeabilities of cultured, well-differentiated normal and cystic fibrosis airway epithelia. *J. Clin. Invest.* 105:1419–1427.
22. Robinson, R. A., and R. H. Stokes. 1968. Electrolyte Solutions. Butterworths, London.
23. Hill, A. E. 2008. Fluid transport: a guide for the perplexed. *J. Membr. Biol.* 223:1–11.
24. Fischbarg, J. 2010. Fluid transport across leaky epithelia: central role of the tight junction and supporting role of aquaporins. *Physiol. Rev.* 90:1271–1290.
25. Larsen, E. H., S. Nedergaard, and H. H. Ussing. 2000. Role of lateral intercellular space and sodium recirculation for isotonic transport in leaky epithelia. *Rev. Physiol. Biochem. Pharmacol.* 141:153–212.
26. Goldman, D. E. 1943. Potential, impedance, and rectification in membranes. *J. Gen. Physiol.* 27:37–60.
27. Danahay, H., H. C. Atherton, …, R. J. Bridges. 2006. Membrane capacitance and conductance changes parallel mucin secretion in the human airway epithelium. *Am. J. Physiol. Lung Cell. Mol. Physiol.* 290:L558–L569.

28. Hille, B. 2001. Ion Channels of Excitable Membranes. Sinauer, Sunderland, MA.

29. Harvey, B. J., and R. P. Kernan. 1984. Sodium-selective microelectrode study of apical permeability in frog skin: effects of sodium, amiloride and ouabain. *J. Physiol.* 356:359–374.

30. Jayaraman, S., Y. Song, and A. S. Verkman. 2001. Airway surface liquid pH in well-differentiated airway epithelial cell cultures and mouse trachea. *Am. J. Physiol. Cell Physiol.* 281:C1504–C1511.

31. Willumsen, N. J., C. W. Davis, and R. C. Boucher. 1994. Selective response of human airway epithelia to luminal but not serosal solution hypertonicity. Possible role for proximal airway epithelia as an osmolality transducer. *J. Clin. Invest.* 94:779–787.

32. Clarke, L. L., and R. C. Boucher. 1992. Chloride secretory response to extracellular ATP in human normal and cystic fibrosis nasal epithelia. *Am. J. Physiol.* 263:C348–C356.

33. Clarke, L. L., T. Chinet, and R. C. Boucher. 1997. Extracellular ATP stimulates $K^+$ secretion across cultured human airway epithelium. *Am. J. Physiol.* 272:L1084–L1091.

34. Manzanares, D., C. Gonzalez, …, M. Salathe. 2011. Functional apical large conductance, $Ca^{2+}$-activated, and voltage-dependent $K^+$ channels are required for maintenance of airway surface liquid volume. *J. Biol. Chem.* 286:19830–19839.

35. Poulsen, A. N., T. L. Klausen, …, O. Frederiksen. 2006. Nucleotide regulation of paracellular $Cl^-$ permeability in natural rabbit airway epithelium. *Pflugers Arch.* 452:188–198.

36. Flynn, A. N., O. A. Itani, …, M. J. Welsh. 2009. Acute regulation of tight junction ion selectivity in human airway epithelia. *Proc. Natl. Acad. Sci. USA.* 106:3591–3596.

37. Dudeja, P. K., N. Hafez, …, F. J. Al-Bazzaz. 1999. Expression of the $Na^+/H^+$ and $Cl^-/HCO_3^-$ exchanger isoforms in proximal and distal human airways. *Am. J. Physiol.* 276:L971–L978.

38. Paradiso, A. M., R. D. Coakley, and R. C. Boucher. 2003. Polarized distribution of $HCO_3^-$ transport in human normal and cystic fibrosis nasal epithelia. *J. Physiol.* 548:203–218.

39. Kreindler, J. L., K. W. Peters, …, R. J. Bridges. 2006. Identification and membrane localization of electrogenic sodium bicarbonate cotransporters in Calu-3 cells. *Biochim. Biophys. Acta.* 1762:704–710.

40. Devor, D. C., R. J. Bridges, and J. M. Pilewski. 2000. Pharmacological modulation of ion transport across wild-type and ΔF508 CFTR-expressing human bronchial epithelia. *Am. J. Physiol. Cell Physiol.* 279: C461–C479.

41. Smith, P. L., and R. A. Frizzell. 1982. Changes in intracellular K activities after stimulation of Cl secretion in canine tracheal epithelium. *Chest.* 81:5S.

42. Smith, P. L., and R. A. Frizzell. 1984. Chloride secretion by canine tracheal epithelium: IV. Basolateral membrane K permeability parallels secretion rate. *J. Membr. Biol.* 77:187–199.

43. Stutts, M. J., C. U. Cotton, …, R. C. Boucher. 1985. Chloride uptake into cultured airway epithelial cells from cystic fibrosis patients and normal individuals. *Proc. Natl. Acad. Sci. USA.* 82:6677–6681.

44. Boucher, R. C., M. J. Stutts, …, J. T. Gatzy. 1981. Regional differences in airway surface liquid composition. *J. Appl. Physiol.* 50:613–620.

45. Coakley, R. D., B. R. Grubb, …, R. C. Boucher. 2003. Abnormal surface liquid pH regulation by cultured cystic fibrosis bronchial epithelium. *Proc. Natl. Acad. Sci. USA.* 100:16083–16088.

46. Lindenmayer, G. E., A. Schwartz, and H. K. Thompson, Jr. 1974. A kinetic description for sodium and potassium effects on ($Na^+$ plus $K^+$)-adenosine triphosphatase: a model for a two-nonequivalent site potassium activation and an analysis of multiequivalent site models for sodium activation. *J. Physiol.* 236:1–28.

47. Miyamoto, H., T. Ikehara, …, T. Masuya. 1986. Kinetic mechanism of $Na^+$, $K^+$, $Cl^-$—cotransport as studied by $Rb^+$ influx into HeLa cells: effects of extracellular monovalent ions. *J. Membr. Biol.* 92:135–150.

48. Battogtokh, D., D. K. Asch, …, H. B. Schuttler. 2002. An ensemble method for identifying regulatory circuits with special reference to the QA gene cluster of *Neurospora crassa*. *Proc. Natl. Acad. Sci. USA.* 99:16904–16909.

49. Levin, M. H., S. Sullivan, …, A. S. Verkman. 2006. Hypertonic saline therapy in cystic fibrosis: evidence against the proposed mechanism involving aquaporins. *J. Biol. Chem.* 281:25803–25812.

50. Li, Y.-H. 1974. Diffusion of ions in sea water and in deep-sea sediments. *Geochim. Cosmochim. Acta.* 38:703–714.

51. Xin, Q., and R. M. Wightman. 1997. Transport of choline in rat brain slices. *Brain Res.* 776:126–132.

52. Zuidema, T., K. Dekker, and J. S. Heukelom. 1985. The influence of organic counterions on junction potentials and measured membrane potentials. *Bioelectrochem. Bioenerg.* 14:479–494.